

## Corrosion Mechanism of Microporous Nickel-Chromium Coatings

### Part II. SECM Study Monitoring $\text{Cu}^{2+}$ and Oxygen Reduction

Ganborena, Larraitz; Gonzalez-Garcia, Yaiza; Özkaya, Berkem; García, Marta; García-Lecina, Eva; Vega, Jesús Manuel

**DOI**

[10.1149/1945-7111/ac554a](https://doi.org/10.1149/1945-7111/ac554a)

**Publication date**

2022

**Document Version**

Final published version

**Published in**

Journal of the Electrochemical Society

**Citation (APA)**

Ganborena, L., Gonzalez-Garcia, Y., Özkaya, B., García, M., García-Lecina, E., & Vega, J. M. (2022). Corrosion Mechanism of Microporous Nickel-Chromium Coatings: Part II. SECM Study Monitoring  $\text{Cu}^{2+}$  and Oxygen Reduction. *Journal of the Electrochemical Society*, 169(2), Article 021509. <https://doi.org/10.1149/1945-7111/ac554a>

**Important note**

To cite this publication, please use the final published version (if applicable).  
Please check the document version above.

**Copyright**

Other than for strictly personal use, it is not permitted to download, forward or distribute the text or part of it, without the consent of the author(s) and/or copyright holder(s), unless the work is under an open content license such as Creative Commons.

**Takedown policy**

Please contact us and provide details if you believe this document breaches copyrights.  
We will remove access to the work immediately and investigate your claim.

***Green Open Access added to TU Delft Institutional Repository***

***'You share, we take care!' - Taverne project***

**<https://www.openaccess.nl/en/you-share-we-take-care>**

Otherwise as indicated in the copyright section: the publisher is the copyright holder of this work and the author uses the Dutch legislation to make this work public.

## Corrosion Mechanism of Microporous Nickel-Chromium Coatings: Part II. SECM Study Monitoring $\text{Cu}^{2+}$ and Oxygen Reduction

To cite this article: Larraitz Ganborena *et al* 2022 *J. Electrochem. Soc.* **169** 021509

View the [article online](#) for updates and enhancements.

### ECS Toyota Young Investigator Fellowship



For young professionals and scholars pursuing research in batteries, fuel cells and hydrogen, and future sustainable technologies.

At least one \$50,000 fellowship is available annually.  
More than \$1.4 million awarded since 2015!




Application deadline: January 31, 2023

**Learn more. Apply today!**



## Corrosion Mechanism of Microporous Nickel-Chromium Coatings: Part II. SECM Study Monitoring $\text{Cu}^{2+}$ and Oxygen Reduction

Larraitz Ganborena,<sup>1</sup> Yaiza Gonzalez-Garcia,<sup>2</sup> Berkem Özkaya,<sup>3</sup> Marta García,<sup>4</sup> Eva García-Lecina,<sup>1</sup> and Jesús Manuel Vega<sup>1,z</sup> 

<sup>1</sup>CIDETEC, Basque Research and Technology Alliance (BRTA), Paseo Miramón 196, 20014 Donostia-San Sebastián, Spain

<sup>2</sup>Delft University of Technology, Department of Materials Science and Engineering, Mekelweg 2, 2628 CD, Delft, The Netherlands

<sup>3</sup>Atotech Deutschland GmbH, Postfach 21 07 80, 10507 Berlin, Germany

<sup>4</sup>MTC—Maier Technology Centre, Polígono Industrial Arabieta, B° Kanpantxu S/N, 48320 Ajangiz-Bizkaia, Spain

The corrosion mechanism of microporous nickel-chromium multilayer coatings was studied at localised scale by Scanning Electrochemical Microscopy (SECM) after exposure to an aggressive electrolyte (chloride-based one at pH 3.1 containing cupric ions). The open circuit potential was initially monitored during 22 h, followed by a detailed characterisation using Glow Discharge-Optical Emission Spectroscopy and Field Emission Scanning Electron Microscope. Interestingly, Cu deposition occurs over the surface of the microporous nickel layer, and it is located on spots where micro-discontinuities (i.e., cracks and pores) of the outermost Cr layer are present. The application of different operation modes of the SECM (i.e., redox competition and surface generation/tip collection) not only reveals such copper deposits (which were identified after monitoring their catalytic capabilities for oxygen reduction reaction) but also confirms the stepwise reduction of  $\text{Cu}^{2+}$  to  $\text{Cu}^0$  (via intermediate species of  $\text{Cu}^+$ ) during the corrosion process. The impact of metallic copper particles in the local pH due to their catalytic activity could also explain why the microporous nickel layer is not corroded after exposure to such electrolyte.

© 2022 The Electrochemical Society ("ECS"). Published on behalf of ECS by IOP Publishing Limited. [DOI: [10.1149/1945-7111/ac554a](https://doi.org/10.1149/1945-7111/ac554a)]

Manuscript submitted November 3, 2021; revised manuscript received February 8, 2022. Published February 23, 2022. *This paper is part of the JES Focus Issue on Women in Electrochemistry.*

Usually, decorative nickel-chromium coatings show the following multilayer configuration from top to bottom: (i) a topmost microporous chromium layer (below 500 nm thickness), (ii) three nickel layers (having different electrochemical potential values) underneath the chromium one, (iii) a copper layer which ensures the adherence between the deepest nickel layer and the substrate, and (iv) a polymeric substrate. The nickel deposits are plated in a configuration where the layer with the lowest potential (called Bright nickel (B Ni)) is located in between the microporous nickel layer (MPS Ni, above) and the semi-bright nickel one (SB Ni, below)<sup>1</sup> (Fig. 1). Such a design leads to the preferential corrosion of the nickel layer with the lowest potential (i.e., B Ni), while maintaining the attractive appearance and good corrosion resistance of these coatings.<sup>2,3</sup>

Nowadays, the industry is using the Copper Accelerated Acetic Acid Salt Spray (CASS) test to evaluate the corrosion performance of such coatings (standard ASTM B368).<sup>4</sup> However, the role of cupric ions has not been explored in detail during the corrosion of these coatings. In general, electrochemical methods<sup>5</sup> and quantum chemical ones<sup>6</sup> have shown the oxidising effect of cupric ions. This behaviour has been widely explored in aluminium and aluminium alloys after exposure to solutions containing  $\text{Cu}^{2+}$  ions<sup>7–10</sup> as well as in the aluminium alloy 2024 after exposure to chloride-based electrolytes.<sup>11</sup> In the latter,  $\text{Cu}^{2+}$  cations are released from the alloy. Its subsequent reduction over Al-Cu-Mn-Fe intermetallic particles (acting as cathodic sites) seems to contribute to overall corrosion (apparently accelerates pitting corrosion).

Recently, it was shown that not only cupric ions increase the corrosion rate of microporous nickel-chromium systems but also affect the aesthetic of the surface.<sup>12</sup> Such visual impact can be related to the degradation of the nickel layers underneath the chromium one. Using  $\text{Cu}^{2+}$ -based electrolytes, it was observed that the only nickel layer affected by corrosion is the bright nickel one. In contrast, the corrosion mechanism is entirely different in the absence of  $\text{Cu}^{2+}$  (i.e., acidified chloride-based electrolyte), leading to the corrosion of all nickel layers: bright nickel > microporous

nickel > semibright nickel.<sup>13</sup> On the other hand, drop tests by Scanning Kelvin Probe (SKP) have confirmed the reduction of cupric to cuprous ions using  $\text{Cu}^{2+}$ -based electrolytes. Only the exposed area to the droplet showed higher potential values (most probably due to the presence of local cathodes).<sup>12</sup>

However, it is still unclear why the presence or absence of cupric ions provokes a change in the corrosion mechanism. Scanning Electrochemical Microscopy (SECM) can be used for studying electrochemical reactions at local scale. SECM is a versatile tool that includes different operation modes, enabling the evaluation of topography and electrochemical activity with high spatial resolution.<sup>14</sup> SECM allows studying different features of corrosion processes such as kinetics,<sup>15</sup> location of anodic and cathodic sites<sup>16</sup> and the self-healing capabilities of polymeric coatings,<sup>17</sup> among others. Generation/Collection (G/C) mode enables monitoring electroactive species (by collecting them) generated during the process of interest. For example,  $\text{Cu}^+$  ions (generated from the reduction of  $\text{Cu}^{2+}$  in a solution with  $\text{CuSO}_4$  and chlorides) have been successfully studied during the electrodeposition of copper by Surface Generation/Tip Collection (SG/TC) SECM.<sup>18</sup> This mode has also been employed to measure the local activity of coated membranes by monitoring the  $\text{Cu}^{2+}/\text{Cu}^+$  redox couple in the electrolyte.<sup>19</sup>

Therefore, this research aims to understand the role of cupric ions to explain the corrosion mechanism of microporous nickel-chromium coatings. Samples were exposed to an electrolyte containing cupric and chloride ions at pH 3.1 (i.e., CASS electrolyte) and characterised by Field Emission Scanning Electron Microscope (FE-SEM) and Glow Discharge-Optical Emission Spectroscopy (GD-OES). SECM was used for studying the corrosion process using two different scenarios: (i) monitoring the reduction of  $\text{Cu}^{2+}$  during the corrosion of fresh (i.e., as obtained) specimens, and (ii) monitoring the electrochemical activity (i.e., oxygen reduction reaction (ORR)) of copper deposits (formed in specimens previously exposed (i.e., post-exposed) to the CASS electrolyte).

### Material and Methods

**Material preparation.**—Two types of samples were prepared from trivalent chromium baths: microporous and non-porous nickel-chromium multilayer coatings (the latter for comparative purposes).

<sup>z</sup>E-mail: [jvega@cidetec.es](mailto:jvega@cidetec.es)

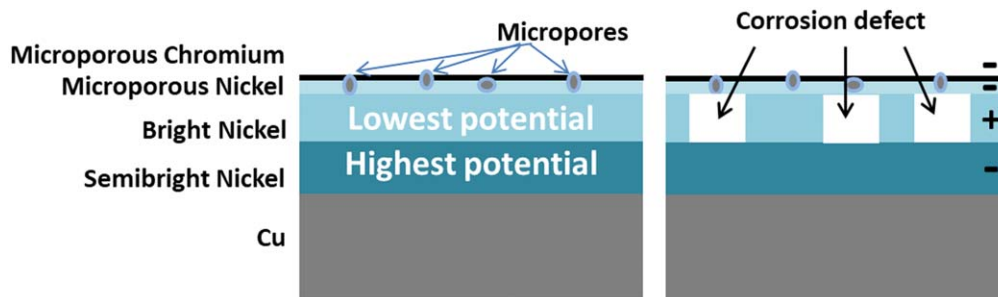


**Figure 1.** (Left) Scheme of a microporous coatings and (right) outcome of the corrosion mechanism of this system in Cu+Cl electrolyte.

The electrodeposition procedure was already described elsewhere<sup>13</sup> using acrylonitrile butadiene styrene (ABS) as the substrate for both systems. The non-porous system was obtained using the same experimental parameters but modifying the formulation of the bath to obtain the MPS Ni layer: i.e., the inert micro-particles (e.g.,  $\text{Al}_2\text{O}_3$ ) were not added in order to avoid the porosity in the MPS Ni layer, and therefore, the presence of pores in the outmost Cr layer.

On the other hand, a 99.95% purity Cu foil (Goodfellow) was used as reference material for the SECM experiments.

Finally, the main electrolyte (labelled as “Cu+Cl electrolyte”) has the same composition as the one used in the CASS test: 0.9 M NaCl + 1.5 mM  $\text{CuCl}_2$ . In order to perform certain SECM measurements, it was modified as follows: (i) 0.9 M NaCl without cupric ions (labeled as “Cl electrolyte”) and (ii) 0.9 M NaCl + 1.5 mM  $\text{CuCl}_2$  + 5 mM  $\text{NiCl}_2 \cdot 6\text{H}_2\text{O}$  (labeled as “Cu+Cl+ $\text{Ni}^{2+}$  electrolyte”). All solutions were prepared with analytical grade reagents and 18.5 M $\Omega$ cm deionised water. The pH of the solution was adjusted to 3.1 by the addition of glacial acetic acid.

**Open circuit potential (OCP) measurements.**—An area of 1 cm<sup>2</sup> was exposed to Cu+Cl electrolyte at 49 °C to simulate the temperature of the CASS test. Open circuit potential (OCP) measurements were performed using a VSP-300 BioLogic potentiostat in a three-electrode flat corrosion cell with Ag/AgCl (3 M KCl) as a reference electrode and a platinum mesh as a counter electrode. Tests were run for 22 h and repeated a minimum of three times, seeking reproducibility.

**Surface characterization.**—The FE-SEM (Gemini Ultraplus from Zeiss) was employed to characterise the surface of both types of samples (microporous and non-porous) and was coupled to an energy dispersive X-ray spectrometer (EDS) to determine the chemical composition. The surface of the microporous nickel layer underneath the chromium one was also explored once the chromium layer was partially or completely removed (Fig. 2 shows the scheme of the stripping process using a solution of HCl:distilled water 1:1).

Elemental depth profiles were obtained by Glow Discharge-Optical Emission Spectroscopy (GD-OES) using a Horiba Jobin-Yvon RF10000 instrument of *post-exposed* samples to the Cu+Cl electrolyte. Measurements were performed at Argon pressure of 650 Pa, 30 W power, an area of 12.5 mm<sup>2</sup>. Data was collected every 10 ms during sputtering. For this particular test and to avoid data distortion due to blistering of the plastic substrate (heated during the

measurement), coatings were plated on brass substrates rather than in ABS. The thickness in the case of the nickel layers was lower than in ABS samples.

**Scanning electrochemical microscope (SECM) experiments.**—M470 electrochemical workstation (BioLogic) was used to perform the SECM measurements. A 15  $\mu\text{m}$  diameter platinum ultramicroelectrode (UME) probe was used with RG-ratio (glass diameter to electrode diameter) of approximately 14.5. Standard saturated calomel electrode (SCE) and platinum foil were employed as the reference and auxiliary electrodes, respectively. All tests were run at room temperature and repeated at least three times for reproducibility.

SECM experiments were carried out on microporous nickel-chromium multilayer samples under two different conditions: (i) *as obtained* (before exposure to any electrolyte), and (ii) *post-exposed* after 22 h of exposure to Cu+Cl electrolyte at 49 °C. The sample area for the SECM experiments was delimited by an adhesive tape (insulator). The area exposed was 0.2 cm<sup>2</sup>.

**SECM: linear sweep voltammetry (LSV) and Cyclic voltammetry (CV).**—In order to identify the redox potential of the different reactions at the UME, LSVs and CVs were carried out in the bulk electrolyte at 5 mVs<sup>-1</sup> scan rate. Although the potential range differed depending on the electrolyte, it was between 0.5 and -0.5 V.

**SECM: approach curves.**—The approach curves were performed over the adhesive tape (insulating material) and the microporous nickel-chromium coatings (active). The SECM probe was placed (using a camera) at a distance close to 200  $\mu\text{m}$  above the surface, and the approach curves were run after 1 h of exposure to the electrolyte. The UME was moved towards the surface by 5  $\mu\text{m}$  steps at a rate of 10  $\mu\text{m s}^{-1}$ .

In the case of the Cu+Cl electrolyte,  $\text{Cu}^{2+}$  ions were used as the redox mediator, whereas in the Cl electrolyte, the dissolved  $\text{O}_2$  was chosen.

The current data were normalised by dividing the tip current by the limiting current ( $i_{\text{norm}} = i/i_{\text{lim}}$ ), and the position dividing the distance by the radius of the UME ( $L_{\text{norm}} = d/a$ ).

**SECM: area scans.**—The sample was under OCP during this type of measurement. Surface area scans (500  $\mu\text{m} \times 500 \mu\text{m}$  dimension)

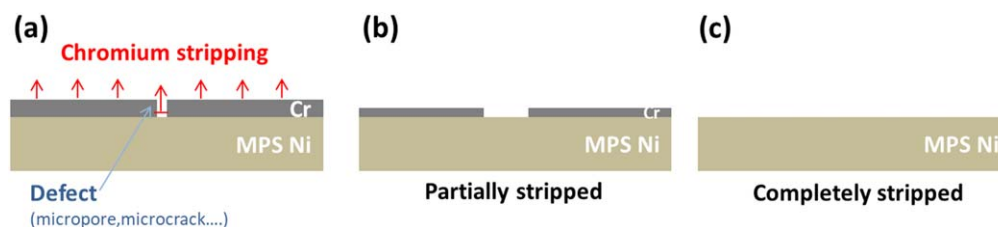


**Figure 2.** Scheme of the stripping process of microporous coatings: (a) initiation of the chemical dissolution of the chromium layer, (b) chromium layer partially stripped (c) chromium layer completely stripped.

were obtained using a scan rate of  $10\ \mu\text{m s}^{-1}$  and steps of  $25\ \mu\text{m}$  to move the tip. In the *Cu+Cl electrolyte*, SECM was operated in competition mode for  $\text{Cu}^{2+}$  detection (Fig. 3a) and SG/TC mode for  $\text{Cu}^+$  (Fig. 3b). A tip to sample distance of  $20\ \mu\text{m}$  was used in the *Cu+Cl electrolyte*. On the other hand, experiments done in the *Cl electrolyte* were performed using the competition mode (Fig. 3a) and with a tip to sample distance of  $30\ \mu\text{m}$ . The distance was increased from  $20\ \mu\text{m}$  to  $30\ \mu\text{m}$  in order to avoid/minimise the effect of a local pH increase promoted by oxygen reduction reaction in the UME.<sup>20</sup>

**SECM: point measurements.**—Point measurements were performed over specific locations/spots using the SG/TC mode. UME was polarised to collect  $\text{Cu}^+$  whilst the sample was transiently polarised (i.e., pulses of 10 s) from the OCP to a potential value able to oxidize  $\text{Cu}^0$  (Fig. 3c).

## Results and Discussion

**Characterisation after exposure to *Cu+Cl electrolyte* by FE-SEM.**—The microporous and non-porous nickel-chromium multilayer samples were exposed to *Cu+Cl electrolyte* at  $49\ ^\circ\text{C}$  for a period of 22 h. Figure 4a shows the typical micro-discontinuities of the chromium coating (*as obtained*) for decorative applications: micropores and microcracks. Micropores are intended discontinuities generated by the co-deposition of non-conductive particles (e. g., alumina) during the electrodeposition of the MPS Ni layer ( $1.40 \pm 0.20\ \mu\text{m}$  thickness). These particles avoid the formation of a continuous chromium layer (around 200 nm thick) due to not being fully integrated into the Ni layer. The electrodeposition of the subsequent chromium layer is hindered at their location, creating a pathway between the outer chromium layer and the underneath layers (i.e., to the MPS Ni layer and the B Ni one). Therefore, porous not only refers to the chromium layer but also the MPS Ni one. Such specimens have microporous as discontinuity at any of these layers (see rhomboid shape, Fig. 4a) compared to the non-porous ones (Fig. 5a). On the other hand, microcracks are a consequence of the electrodeposition process. During the chromium plating process, hydrogen evolution from the reduction of protons promotes the formation of microcracks in the chromium layer.<sup>21</sup>

Samples were also analysed by FE-SEM after exposure to *Cu+Cl electrolyte*. Layers are galvanically coupled in order to improve the corrosion resistance of the overall multilayer system. The corrosion front is guided to the B Ni layer to maintain the aesthetic on the surface of the chromium coating.<sup>2,22</sup> In agreement with our previous studies using similar samples, the surface of the decorative chromium layer is free of corrosion products.<sup>12</sup> In fact, a protective oxide layer is formed.<sup>23</sup> Therefore, to further explore the effect of cupric ions underneath the chromium layer, this topmost layer was

chemically stripped to reveal the surface of the MPS Ni layer. Figures 4c and d show the surface of stripped samples after 3.5 h and 22 h of exposure, respectively.

Interestingly, a single micropore (black area) is showing particles all around its edge (Fig. 4c). It also shows a thread of particles that goes from the edge of a single micropore towards a pore-free surface area. If the exposure time is increased, a similar finding was observed in Fig. 4d, where particles are also present in defect-free areas. Such deposits become more evident due to the discrete particles, ranging from 100 to 200 nm diameter, being arranged in rows over the surface of the MPS Ni layer. The chemical composition of such particles was determined by EDS point analysis in several spots using Ni (from the MPS Ni layer) as a counterbalancing element. The atomic percentage of copper deposits varies from 20 to 74 atomic %. The different compositions from particle to particle can be explained by the difference in diameter/size, affecting the depth reached by the EDS beam.<sup>24</sup> It is interesting to point out that chloride was not detected in the compositional analysis of the particles. Cupric ion in a chloride electrolyte undergoes a stepwise reduction to  $\text{Cu}^+$  and later to copper ( $\text{Cu}^0$ )<sup>25,26</sup> where chloride ions stabilise cuprous anions by the formation of complexes. Previous results indirectly confirmed the formation of  $\text{Cu}^+$  due to the precipitation of  $\text{CuCl}$  in the SKP chamber using the same coatings.<sup>12</sup> Therefore, according to the findings in Fig. 4, the reduction process of  $\text{Cu}^{2+}$  could lead to  $\text{Cu}^+$  species and to the deposition of metallic copper. In order to know the effect of pores as well as understand the noticeable arrangement of Cu particles in threads, non-porous coatings were also characterised. Figure 5a shows the surface of a non-porous sample (pore-free) before exposure (i.e., *as obtained*), having only cracks as microdiscontinuity. If the chromium layer is partially stripped on *post-exposed* coatings (Fig. 6b) and compared to Fig. 4d, similar particles distribution and composition was found into wide microcracks. Considering that the primary cathodic reaction in the corrosion mechanism of these coatings in *Cu+Cl electrolyte* is the  $\text{Cu}^{2+}$  reduction,<sup>13</sup> the copper precipitation seems to be taking place over the MPS Ni layer either through microcracks or micropores. The presence of copper deposits over the microporous nickel layer could justify the protection of such a layer compared to bright nickel (acting as the anode).<sup>27</sup>

**Characterisation after exposure to *Cu+Cl electrolyte* by GD-OES.**—Depth profiles measurements were carried out to determine whether copper deposits are found in the different nickel layers or not. Figure 6 shows the compositional depth profiles of *post-exposed* samples by GD-OES. The depth profile of four different elements (Cr, Ni, Cu and S) was obtained. For the sake of comparison, Cu and

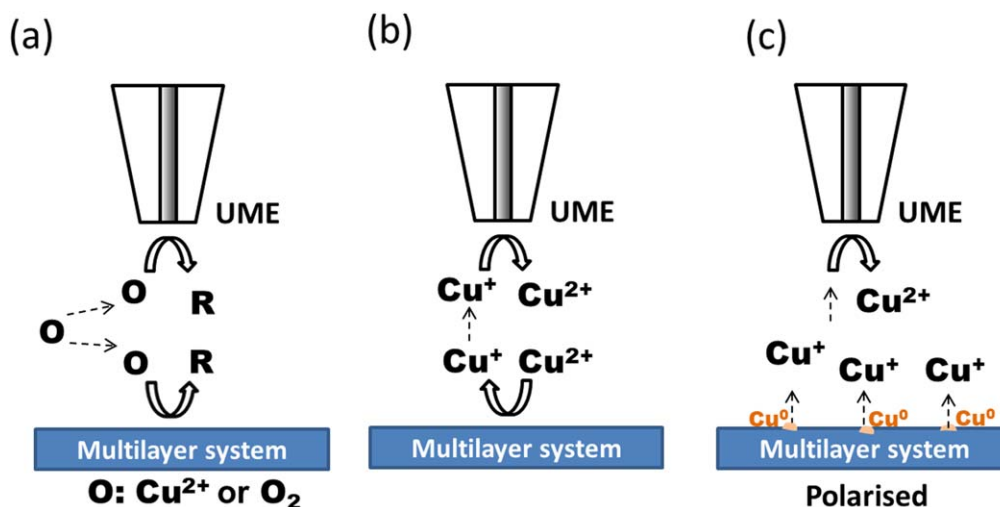


**Figure 3.** SECM operation modes: (a) competition, (b) SG/TC and (c)  $\text{Cu}^+$  SG/TC by sample transient polarisation.



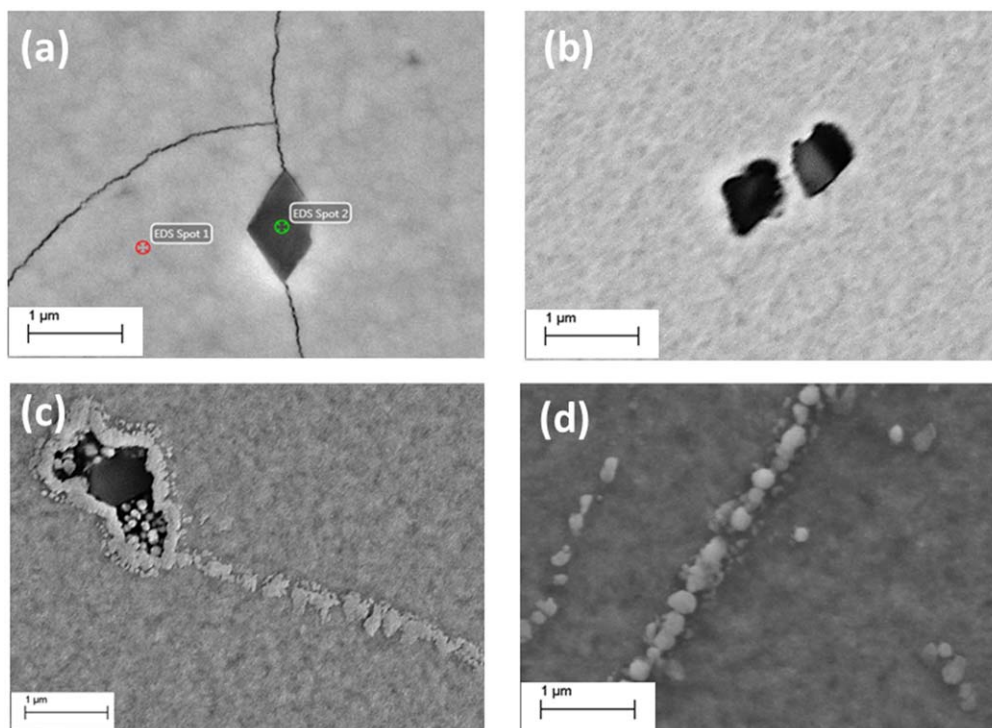


**Figure 4.** FE-SEM micrographs of the surface of microporous coatings exposed to Cu+Cl electrolyte: (a) before exposure (*as obtained*), (b) stripped before exposure, (c) stripped after 3.5 h of exposure, and (d) stripped after 22 h of exposure (*post-exposed*).

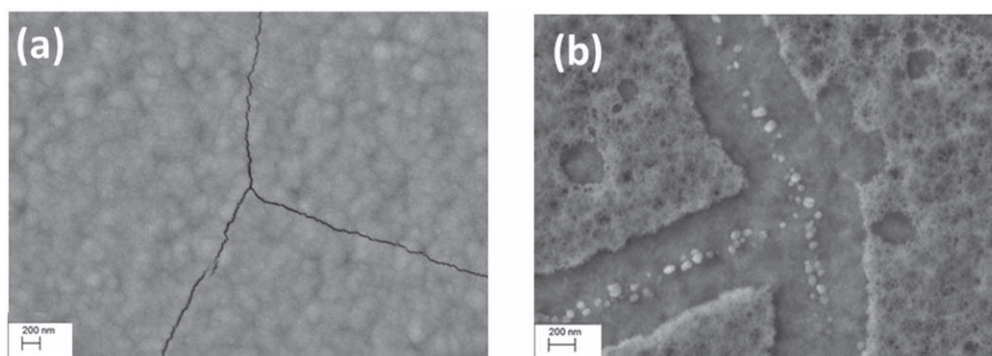


**Figure 5.** FE-SEM micrographs of the surface of non-porous coatings exposed to Cu+Cl electrolyte: (a) before exposure to the electrolyte (*as obtained*), and (b) partially stripped after 22 h of exposure (*post-exposed*).

S data were multiplied by a factor of 100. The boundary between different nickel layers was estimated based on the S content (B Ni layer has the highest concentration) present in certain brightening additives. In agreement with FE-SEM micrographs (Figs. 4c and 4d), results have shown that copper was preferentially present in the MPS Ni layer (it was around 0.6% up to 1  $\mu\text{m}$  depth) and its concentration suddenly decreased (to 0.35% beyond 1  $\mu\text{m}$  depth) once the B Ni layer is reached. Finally, Cu becomes negligible (below the detection limit) beyond 4.5  $\mu\text{m}$  depth. Therefore, although a certain amount of copper was detected in the B Ni layer, it can be assumed that copper is mainly along with the MPS Ni layer.

**Monitoring the  $\text{Cu}^{2+}$  reduction by SECM.**—SECM was used to study the reduction reaction of cupric ions during the corrosion process of microporous nickel-chromium coatings. As mentioned before, the presence of  $\text{Cu}^{2+}$  ions in the electrolyte can enhance the cathodic process during the corrosion process of microporous nickel-chromium coatings by the  $\text{Cu}^{2+}$  reduction reaction to  $\text{Cu}^+$ , which is a different corrosion mechanism than the one during immersion in Cl electrolyte.<sup>13</sup> The SECM was used to prove that the reduction of

$\text{Cu}^{2+}$  takes place. For this, the microelectrode was polarised at specific potentials to monitor the depletion of  $\text{Cu}^{2+}$  in solution and the enrichment of  $\text{Cu}^+$  ions, both processes a consequence of the corrosion cathodic process involving Cu+Cl solution.

#### **Determination of the potential of the SECM microelectrode.**—

To determine the potential at which the reduction of  $\text{Cu}^{2+}$  occurs, voltammetry experiments were carried out in the bulk Cu+Cl electrolyte. Figure 7 shows the CV (from 0.5 V to  $-0.12$  V) of the UME. The onset potential for  $\text{Cu}^{2+}$  reduction to  $\text{Cu}^+$  was observed at 0.3 V by detecting a reduction current.<sup>25,26</sup> A limiting current was reached from 0.1 V to  $-0.25$  V, indicating that the  $\text{Cu}^{2+}$  reduction reaction to  $\text{Cu}^+$  was under diffusion control. Therefore, cupric ions reduction to cuprous ones could be either directly or indirectly monitored by two modes of the SECM: (i) competition and (ii) SG/TC. In the first approach, the sample and the UME are competing for  $\text{Cu}^{2+}$  ions: the probe is polarised to 0.020 V (potential at which  $\text{Cu}^{2+}$  reduction has reached the limiting current in Fig. 7). In this mode, if the probe measures lower current values, it indicates that the sample is consuming  $\text{Cu}^{2+}$  and there are less Cu available to be

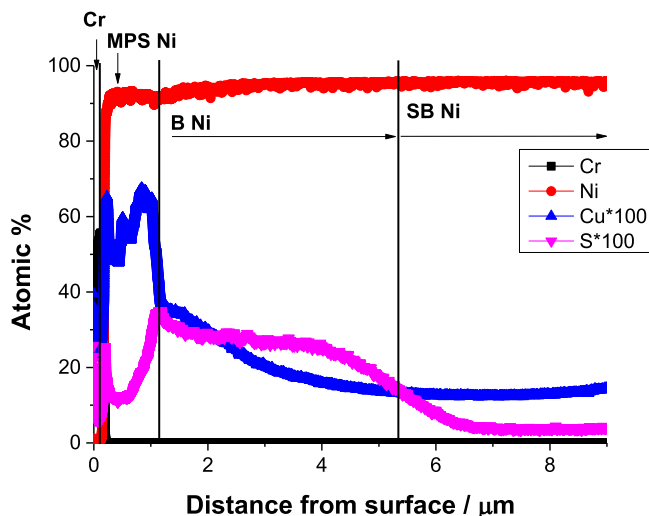


**Figure 6.** GD-OES elemental depth profile for microporous nickel-chromium coatings after 22 h of exposure to Cu+Cl electrolyte (*post-exposed*). Layers indications: Cr (chromium), MPS Ni (microporous nickel), B Ni (Bright nickel) and SB Ni (Semibright nickel).

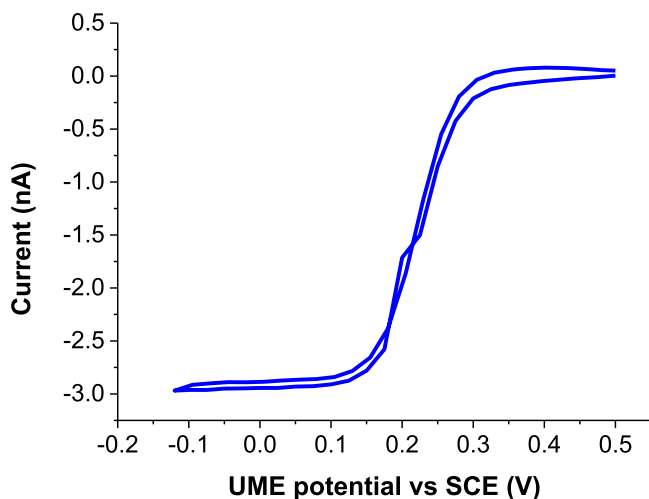


**Figure 7.** CV from 0.5 V to -0.12 V of the Cu+Cl electrolyte at the UME (no sample/substrate here).

reduced at the tip of the UME. In the second approach (i.e., SG/TC mode), the probe has to be polarised at a potential where  $\text{Cu}^+$  is oxidised to  $\text{Cu}^{2+}$  (0.40 V for this research, Fig. 7). Then, the reduction of  $\text{Cu}^{2+}$  by the sample has been indirectly measured by  $\text{Cu}^+$  oxidation in the UME.

**SECM approach curve experiments.**—Figure 8 shows normalised approach curves in Cu+Cl electrolyte for both the sample and the insulator tape surrounding it. As expected, the insulator exhibits the behaviour of a non-active substrate, showing a strong negative feedback response. In fact, when the microelectrode was close to the surface (distances lower to  $L_{\text{norm}} = 7.5$ ), a sharp decrease of current was observed due to the  $\text{Cu}^{2+}$  diffusion towards the tip is hindered by geometrical factors. However, approach curves over the microporous nickel-chromium sample have shown a completely different behaviour: current decreases at distances larger than  $L_{\text{norm}} = 7.5$ . The probe and the substrate are competing for  $\text{Cu}^{2+}$  which can be reduced by the sample due to the corrosion process itself.<sup>13</sup> It implies that the  $\text{Cu}^{2+}$  concentration decreases in the solution and, as a result, lower current values are measured by the tip. Once again, when the UME was too close to the sample, at distances smaller than

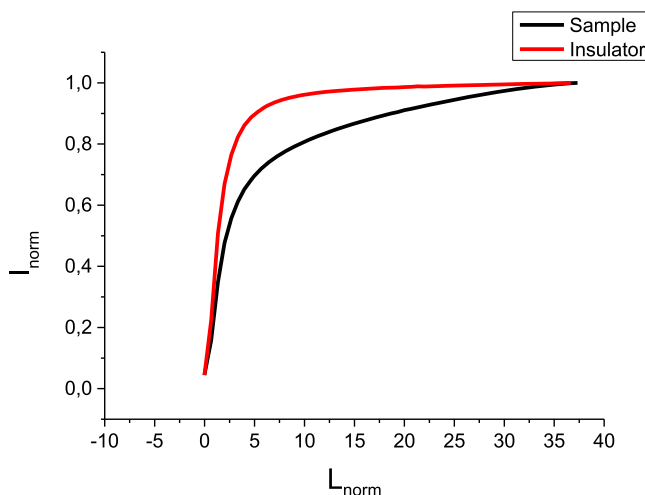


**Figure 8.** Comparison of approach curves towards microporous coatings (black line) and the insulating substrate (red line) with  $\text{Cu}^{2+}$  redox mediator and potential of 0.020 V in Cu+Cl electrolyte.

$L_{\text{norm}} = 7.5$ , the geometrical factor became more apparent, and a sharp current decrease was observed.<sup>20</sup>

**Monitoring the  $\text{Cu}^{2+}$  reduction by SECM area scans.**—Measurements were performed after 2 h of exposure with the coating under OCP. The corrosion process was monitored by SECM following the  $\text{Cu}^{2+}$  reduction reaction using two operation modes: (i)  $\text{Cu}^{2+}$  competition mode at 0.02 V (Fig. 9a), and (ii)  $\text{Cu}^+$  SG/TC mode at 0.4 V (Fig. 9b). Area scans were obtained one after another. Figure 9a shows the  $\text{Cu}^{2+}$  reduction current. The lowest reduction current (below 0.5 nA) indicates a lower amount of  $\text{Cu}^{2+}$  available to be reduced by the probe, and therefore, higher cathodic activity from the sample.

On the other hand, Fig. 9b shows the  $\text{Cu}^+$  oxidation current (positive sign with values between 1.1 – 1.24 nA). In this case, the same area shows higher oxidation currents, indicating a higher concentration of  $\text{Cu}^+$  available to be oxidised by the probe (i.e., large cathodic activity triggering the reduction of  $\text{Cu}^{2+}$  to  $\text{Cu}^+$  ions). This finding was already observed and described during droplet experiments using the SKP, where the formation of  $\text{Cu}^+$  chloride complexes ( $\text{CuCl}_{\text{complex}}$ ) in the electrolyte was proven.<sup>12</sup>

In agreement with the findings in the approaching curves (Fig. 8), these measurements also confirm that the corrosion process has already started after 2 h of immersion. Both SECM maps have shown localised cathodic activity on the surface due to the reduction of  $\text{Cu}^{2+}$  to  $\text{Cu}^+$ , respectively. It seems that the surface presents preferential zones for the cathodic reaction. The local activity became even more localised after longer immersion times (image not shown). This observation agrees with the following hypothesis established in previous work<sup>12</sup>: according to the local increase of potential observed in *post-exposed* samples by SKP, copper particles could be acting as localised cathodes.<sup>12</sup> Nevertheless, from these SECM experiments, we cannot directly attribute the high cathodic activity to the presence of copper particles on the surface. Therefore, the SECM experiment below has been defined to provide more insight about the presence of copper particles which are assumed to modify the corrosion mechanism in Cu+Cl electrolyte compared to Cl-based ones.<sup>13</sup>

**Monitoring the activity of the copper particles by SECM experiments.**—In this section, SECM experiments were designed to confirm the presence of Cu particles deposits on *post-exposed* samples and prove that these deposits can act as local cathodes (i.e., catalytic areas) to reduce oxygen (ORR).<sup>28,29</sup>

The SECM experiments were carried out in the Cl electrolyte. The SECM competition mode was used to seek areas with high ORR



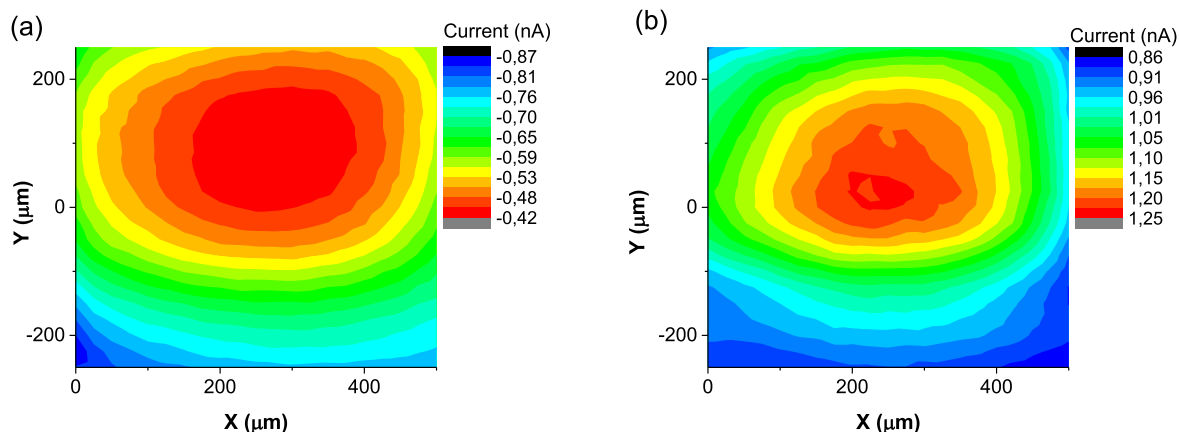


**Figure 9.** SECM maps of microporous coatings after 2 h immersion in Cu+Cl electrolyte: (a) competition mode, and (b) SG/TC mode, measuring  $\text{Cu}^{2+}$  reduction and  $\text{Cu}^+$  generation, respectively. The UME was polarised at (a) 0.020 V and (b) 0.400 V, respectively, depending on the reaction to be monitored.

activity as local cathodes. The SECM SG/TC mode was used to confirm that these locations correspond to copper deposits. In the latter, the sample was polarised at a potential able to oxidise the copper particles ( $\text{Cu}^0$ ) on the surface. Simultaneously, the UME was polarised to detect the formation of  $\text{Cu}^+$  in that location/spot.

**Determination of the ORR potential in the UME.**—Linear voltammetry was carried out to select the potential for monitoring the ORR with the UME. Figure 10 shows the LSV (from 0.5 V to  $-0.5$  V) at the probe in the bulk of the Cl electrolyte. Although the limiting current was nearly reached in the potential range from  $-0.05$  to  $-0.4$  V, a certain  $\text{O}_2$  reduction current was measured around 0.29 V. The onset of a new reduction process was observed to more negative potential values, which corresponds to hydrogen evolution (by the reduction of protons). Therefore,  $-0.25$  V (where almost a limiting current for ORR is reached) was chosen for polarising the UME to compete with the sample for oxygen consumption.

**Determination of the potential to polarise the sample.**—In order to determine the potential to oxidise  $\text{Cu}^0$ , cyclic voltammetry was performed on a plate of Cu (i.e., sample) using the Cl electrolyte. Figure 11a shows a large anodic peak from  $-0.12$  V to 0 V as a consequence of  $\text{Cu}^0$  dissolution to  $\text{Cu}^+$  ions, whereas in the reverse scan, the reduction of  $\text{Cu}^+$  to  $\text{Cu}^0$  is identified at potentials close to  $-0.17$  V.<sup>25</sup> Therefore,  $-0.08$  V was found as a suitable potential value to polarise the sample to trigger the oxidation of  $\text{Cu}^0$ .

The interference of  $\text{Ni}^{2+}$  ions in the detection of  $\text{Cu}^+$  by the probe was discarded according to the results obtained in Fig. 11b. It shows the CV of both electrolytes, Cu+Cl and Cu+Cl+ $\text{Ni}^{2+}$ , where  $\text{Ni}^{2+}$  did not interfere with the redox reaction of copper cations ( $\text{Cu}^+$  oxidation/ $\text{Cu}^{2+}$  reduction).

**Monitoring the activity of the copper particles by SECM area scans.**—SECM area scans were conducted in *post-exposed* samples under OCP, polarising the UME to  $-0.250$  V. ORR in the UME promotes the increase of the pH locally and can affect the corrosion process under study.<sup>20</sup> In order to minimise that effect, the distance from the probe to the sample was  $30\ \mu\text{m}$ .

Figure 12a shows the area scan after 1 h of exposure to the Cl electrolyte. The current values (negative) are uniform along the surface, except for a specific local area of the sample (located approximately at X:225  $\mu\text{m}$ , Y:175  $\mu\text{m}$ ) which exhibits high ORR activity (i.e., low current values were measured by the UME). In order to identify whether or not copper particles deposits are present in that location, the sample was polarised by pulses once the UME was placed over that specific spot (X:225  $\mu\text{m}$ , Y:175  $\mu\text{m}$  coordinates). The goal was to detect the formation of  $\text{Cu}^+$  by SG/TC mode (with the probe polarised at 0.4 V) in such a specific spot.

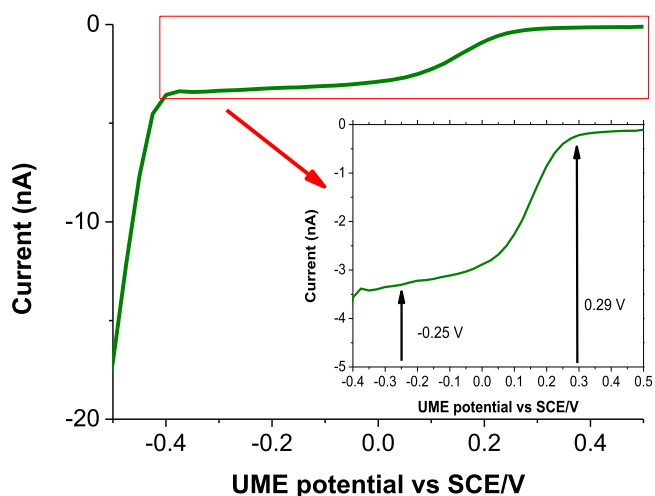


**Figure 10.** LSV from 0.5 V to  $-0.5$  V of the Cl electrolyte at the UME (no sample/substrate here).

Figure 12b shows the current values measured by the UME during the transient polarisation of the sample. At OCP (the initial 30 s), the UME in  $\text{Cu}^+$  SG/TC mode is measuring a baseline current (lower than 0.1 nA). However, when polarising the sample (from 30 to 40 s), the current related to  $\text{Cu}^+$  oxidation increases to 1.6 nA. It gradually decreases during the pulse up to 1.0 nA. Once the pulse was stopped, the current measured by the UME diminished and nearly reached the initial current baseline (beyond 45 s). After a few pulses, no  $\text{Cu}^+$  oxidation current was measured by the UME, pointing out that the complete dissolution of the Cu particles had already taken place.

Therefore, results in Fig. 12 confirmed that  $\text{Cu}^0$  particles/deposits formed during exposure to Cu+Cl electrolyte (Fig. 4) show a higher ORR activity, acting as local cathodes as suggested before.<sup>12</sup> This catalytic activity could be locally increasing the pH and, if exceeding pH 4,<sup>30</sup> could even promote the passivation of the MPS Ni layer.

**Impact of copper deposits in the corrosion mechanism.**—The multilayer configuration of microporous nickel-chromium systems is designed to guide the corrosion front to the B Ni layer. The main goal is to keep the corrosion hidden and preserve the aesthetic appearance of the topmost chromium layer. If these systems are exposed to Cl electrolyte, the corrosion front is not only focused on the bright nickel layer but also affects the microporous nickel layer (and even the SB Ni layer to a lower extent).<sup>13</sup> Therefore, it seems that under this aggressive environment, the difference in

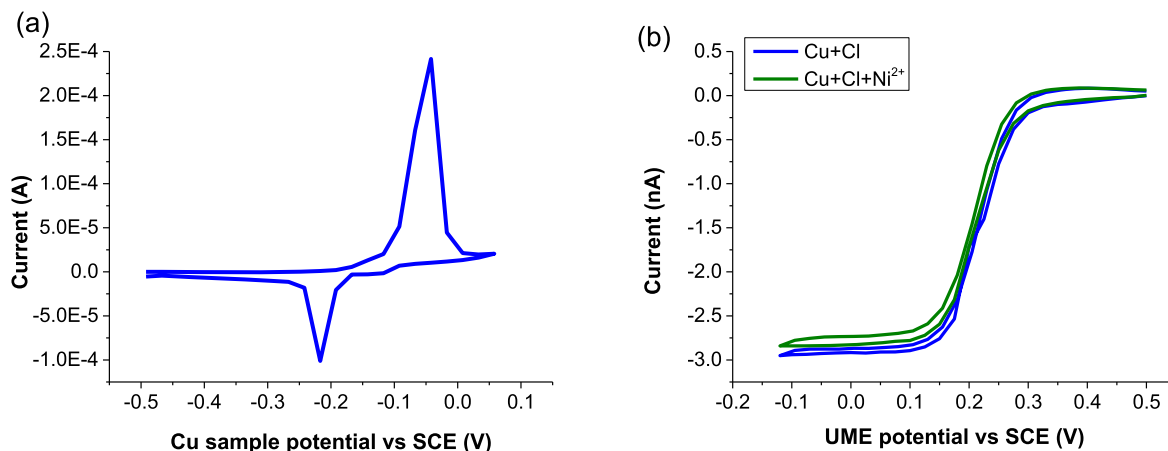


**Figure 11.** (a) CV from  $-0.5$  V to  $0.1$  V of a Cu plate in the Cl electrolyte, and (b) CV from  $0.5$  V to  $-0.12$  V of Cu+Cl electrolyte with and without  $\text{Ni}^{2+}$  at the UME (no sample/substrate here).

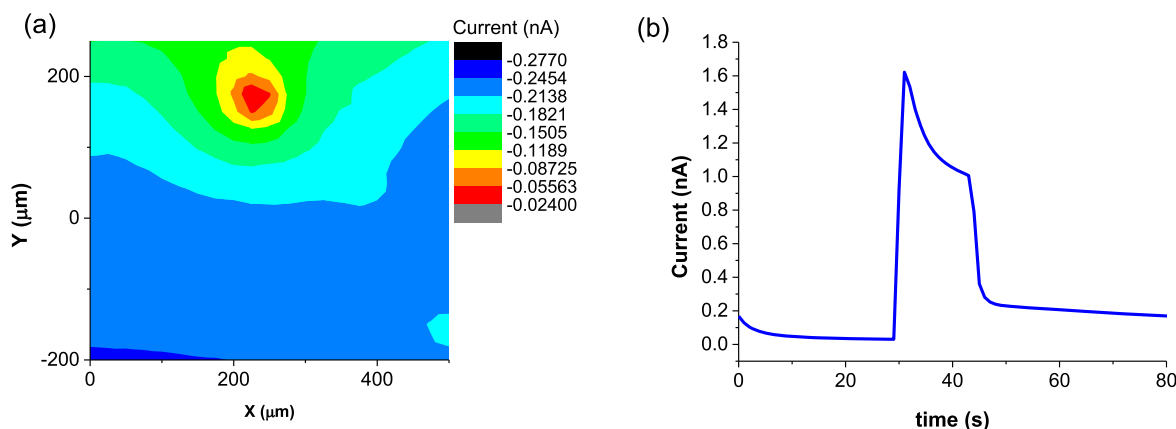


**Figure 12.** SECM images of *post-exposed* microporous coatings in a Cl electrolyte: (a) map obtained in competition for  $\text{O}_2$  consumption, and (b) point measurement over the red spot for  $\text{Cu}^+$  detection (locating the UME in the area with higher oxygen-consuming). The UME was polarised at  $0.400$  V whilst the sample was polarised by pulses to  $-0.080$  V to oxidise the copper particles.

electrochemical potentials between the distinct nickel layers cannot be maintained with time. Considering that the ORR is mainly governing the cathodic reaction, changes in oxygen concentration (e.g., depletion<sup>31–33</sup>) during the corrosion process may diminish such difference of potential, favouring the corrosion of the MPS Ni layer.<sup>13</sup>

In contrast, the corrosion mechanism is drastically changed if these microporous nickel-chromium samples are exposed to *Cu+Cl electrolyte*. It has to be considered that the cathodic reaction is governed by the reduction of cupric ions to  $\text{Cu}^0$  via two single-electron steps. The first step leads to the reduction from  $\text{Cu}^{2+}$  to  $\text{Cu}^+$ , indirectly visualised by the SKP (droplet tests)<sup>12</sup> and identified by the cathodic loops in the polarisation curves of MPS Ni and SB Ni layers.<sup>13</sup> The second stage leads to the preferential deposition of copper (from  $\text{Cu}^+$  to  $\text{Cu}^0$ ) particles over MPS Ni layer.

Both stages have been confirmed by SECM results, either using redox competition and SG/TC modes. During the SECM experiments, the reduction reactions (for Cu-ions and dissolved oxygen) were measured by polarising the UME at selected potentials. This approach was an indirect way to identify and to monitor the cathodic sites occurring during corrosion. It has been confirmed that the  $\text{Cu}^+$  reduction occurs in the areas where the nickel layer (e.g., MPS Ni) is exposed (the electrolyte can diffuse here through micro-discontinuities of the outermost Cr-layer). It explains the localised nature of the activities detected by the SECM. Nevertheless, the spatial dimensions of these activities do not directly reflect the size of the defects or Cu particles agglomerates. The measured currents by the

UME are associated to the concentration of species present in the electrolyte at the proximities of those surface features. Furthermore, due to the stochastic nature of the corrosion process and the experimental setup, it was not possible to associate the local activity detected by the UME with a particular defect on the surface after post-mortem examination of the sample.

Beyond the early findings indicating that the corrosion front is located into the B Ni layer,<sup>2,6</sup> not only the formation of copper deposits on the surface of MPS Ni layer was shown here (a stepwise process), but also the catalytic activity (for ORR) of such deposits was proven. The protection of this layer may lie in the presence of particle/precipitates on the surface which might have an impact on the electrochemical behaviour of the MPS Ni layer, avoiding the polarity reversal between it and the B Ni layer.<sup>13</sup> Such protection could be justified by:

- (i) The formation of a protective layer based on cuprous chloride complexes could inhibit the dissolution of the microporous nickel layer similarly to other materials (e.g., stainless steel or chalcopyrite).<sup>34,35</sup>
- (ii) The passivation of the MPS Ni layer. According to the low pH (3.1) in the electrolyte, none of the bare nickel layers exposed are supposed to be passivated. However, the copper particles can act as local microcathodes (e.g., catalysing the ORR<sup>10,28,29</sup>), increasing the pH locally ( $\text{pH} > 4$ )<sup>30</sup> to protect the surface of the microporous nickel layer.

## Conclusions

Results have shown the versatility and resolution of SECM to investigate complex corrosion processes where several reactions can take place on different metallic layers (i.e., chromium or nickel ones). In this work, we have applied the SECM technique operating in different modes and following novel approaches to explore the impact of cupric ions in the corrosion mechanism of microporous nickel-chromium coatings at a localised scale. The main findings are the following:

- Copper deposits were found on the surface of the microporous nickel layer, and they were mainly located on spots where discontinuities of the outermost chromium layer are present (i.e., microcracks and micropores).
- SECM has been able to show the  $\text{Cu}^{2+}$  stepwise reduction to  $\text{Cu}^0$  during the corrosion process: i) directly by in situ measurement of  $\text{Cu}^{2+}$  reduction to  $\text{Cu}^+$  (competition and SG/TC modes), and ii) indirectly by the oxidation of  $\text{Cu}^0$  deposits to  $\text{Cu}^+$  after applying transient pulses (SG/TC mode able to detect the formation of  $\text{Cu}^+$ ).
- $\text{Cu}^0$  particles have shown their ORR catalytic activity, acting as localised cathodes on the top of the microporous nickel layer. It implies a local increase of the pH at the proximity of the  $\text{Cu}^0$  particles that could explain the protection (e.g., passivation) of the microporous nickel layer in a  $\text{Cu}+\text{Cl}$  electrolyte.

## Aknowledgments

The authors would like to thank the financial support and samples provided by ATOTECH Deutschland GmbH team's. This work was partially supported by Basque government (ELKARTEK, KK-2020/00108) and by the Spanish Government (PID2020-116844RB-C22 and CER-20191003). Dr Yaiza Gonzalez-Garcia acknowledges the funding from COST (European Cooperation in Science and Technology) to carry out an STSM within the framework of the COST action MP 1407.

## ORCID

Jesús Manuel Vega  <https://orcid.org/0000-0001-7944-6520>

## References

1. G. A. Di Bari, *Modern Electroplating* 5th ed., p. 79 (2010).
2. R. Tremmel, *Plat. Surf. Finish.*, **83**, 24 (1996).
3. D. L. Snyder, *Met. Finish.*, **110**, 14 (2012).
4. ASTM B 368 - 21. *Standard Test Method for Copper-Accelerated Acetic Acid-Salt Spray ( Fog ) Testing (CASS Test)*, (2021).
5. G. A. Petrocelli, J. V. Hospadaruk, and V. Dibari, *Plating*, **49**, 50 (1962).
6. R. Schmidt, K. O. Thiel, F. Von Horsten, C. Spickermann, G. Vazhenin, N. Bäumle, P. Wachter, P. Hartmann, and H. J. Schreier, *Mater. Corros.*, **65**, 959 (2014).
7. M. G. A. Khedr and A. M. S. Lashien, *Corros. Sci.*, **33**, 137 (1992).
8. K. S. N. Murthy, R. Ambat, and E. S. Dwarakadasa, *Corros. Sci.*, **36**, 1765 (1994).
9. V. Uksiene, K. Leinartas, R. Juškenas, A. Sudavičius, and E. Juzeliūnas, *Electrochem. Commun.*, **4**, 747 (2002).
10. M. Chiba, Y. Nakayama, T. Hiraga, H. Takahashi, and Y. Shibata, *Surf. Interface Anal.*, **45**, 1626 (2013).
11. H. M. Obispo, L. E. Murr, R. M. Arrowood, and E. A. Trillo, *J. Mater. Sci.*, **5**, 3479 (2000).
12. L. Ganborena, J. M. Vega, B. Özkaya, H. J. Grande, and E. García-Lecina, *Electrochim. Acta*, **318**, 683 (2019).
13. L. Ganborena, B. Özkaya, M. García, H.-J. Grande, E. García-Lecina, and J. M. Vega, *J. Electrochem. Soc.*, **169**, 021503 (2022).
14. J. Kwak and A. J. Bard, *Anal. Chem.*, **61**, 1794 (1989).
15. C. Nowierski, J. J. Noël, D. W. Shoesmith, and Z. Ding, *Electrochem. Commun.*, **11**, 1234 (2009).
16. A. C. Bastos, A. M. Simões, S. González, Y. González-García, and R. M. Souto, *Electrochem. Commun.*, **6**, 1212 (2004).
17. Y. González-García, J. M. C. Mol, T. Muselle, I. De Graeve, G. Van Assche, G. Scheltjens, B. Van Mele, and H. Terryn, *Electrochem. Commun.*, **13**, 169 (2011).
18. A. P. O'Mullane, A. K. Neufeld, and A. M. Bond, *J. Electrochem. Soc.*, **155**, 538 (2008).
19. M. Nebel, S. Neugebauer, H. Kiese, and W. Schuhmann, *Electrochim. Acta*, **55**, 7923 (2010).
20. L. C. Abodi, Y. Gonzalez-Garcia, O. Dolgikh, C. Dan, D. Deconinck, J. M. C. Mol, H. Terryn, and J. Deconinck, *Electrochim. Acta*, **146**, 556 (2014).
21. D. B. Lee, *Mater. Corros.*, **59**, 598 (2008).
22. M. Barnstead, J. Schweitzer, and W. Schumacher, *Plat. Surf. Finish.*, **30** (2010).
23. J. León, S. Pletincx, H. Terryn, B. Özkaya, E. García-Lecina, and J. M. Vega, *J. Electrochem. Soc.*, **168**, 121501 (2021).
24. A. A. El Warraky, A. M. El Aziz, K. A. Soliman, A. A. El Warraky, and K. A. Soliman, *Anticorros. methods Mater.*, **54**, 163 (2007).
25. C. P. De Leon and F. C. Walsh, *Trans. Inst. Met. Finish.*, **81**, 95 (2003).
26. H. Zhao, J. Chang, A. Boika, and A. J. Bard, *Anal. Chem.*, **85**, 7696 (2013).
27. G. S. Chen, M. Gao, and R. P. Wei, *Corrosion*, **52**, 8 (1996).
28. M. Kendig and S. Jeanjaquet, *J. Electrochem. Soc.*, **149**, B47 (2002).
29. M. B. Vukmirovic, N. Vasiljevic, N. Dimitrov, and K. Sieradzki, *J. Electrochem. Soc.*, **150**, B10 (2003).
30. N. Hernández, R. Moreno, A. J. Sánchez-Herencia, and J. L. G. Fierro, *J. Phys. Chem. B*, **109**, 4470 (2005).
31. L. Pohlmann, G. Bauer, P. Hartmann, P. Wachter, and C. Donner, *J. Solid State Electrochem.*, **17**, 489 (2013).
32. G. N. Flint and S. H. Melbourne, *Trans. IMF*, **38**, 35 (1961).
33. G. S. Frankel, *J. Electrochem. Soc.*, **145**, 2186 (1998).
34. Q. Liu, M. Chen, and Y. Yang, *Electrochim. Acta*, **253**, 257 (2017).
35. A. A. Hermas, K. Ogura, and T. Adachi, *Electrochim. Acta*, **40**, 837 (1995).